Finite Wavetrains in a One-Dimensional Medium

C. Kahlert and O. E. Rössler

Institute for Physical and Theoretical Chemistry, University of Tübingen

Z. Naturforsch. **38 a**, 648–667 (1983); received March 12, 1983

A modified Rinzel-Keller equation of reaction-diffusion type is investigated analytically. Both on the ring and on the linear fiber, the possible existence of wavetrains containing an arbitrary finite number of impulses is demonstrated. The longest wavetrain shown explicitly consists of ten pulses. Unlike other approaches, the present method varies many parameters simultaneously. An implicit algebraic equation is formulated which contains all possible wave solutions of the system. This equation is then solved with a standard technique (Powell's algorithm). The results obtained extend the findings of other authors. The method can be applied, after appropriate modification, to other piecewise linear systems, that is, to other prototype reaction-diffusion systems.

1. Introduction

Excitable media include the nerve fiber, the heart surface, the protozoan membrane, a reaction tank containing the Z-reagent, as well as certain ecological (epidemiological) and economic systems. They are all capable of showing spatially homogeneous excitations as well as spatially inhomogeneous excitations called trigger waves [1]. Such waves can be used to explain the transport of information in biological systems, or the occurrence of repetitive and nonrepetitive epidemiological and economic phenomena. In two dimensions a very complicated recurrent behavior was found recently [2].

One possible implementation of an excitable system is a spatially extended medium in which several chemical reactions take place. Some or all of the reactants may be subjected to diffusion. This class of systems can be described by parabolic differential equations which are therefore frequently called "reaction-diffusion equations" (cf. [3]). The most celebrated biological example is the Hodgkin-Huxley equation of nerve action [4]. It is a complicated four-variable nonlinear partial differential equation with diffusion-type coupling.

In the following, a much simpler equation – simple enough to be treated analytically – will be considered. Despite its simplicity, it nonetheless possesses interesting solutions. Wavetrains of more than two pulses in a reaction-diffusion system can be explicitly demonstrated for the first time.

Reprint requests to C. Kahlert, Institut für Physikalische und Theoretische Chemie der Universität Tübingen, Auf der Morgenstelle 8, 7400 Tübingen.

2. The Local System

A straightforward way to obtain excitability in a (local) reaction system is to have one Z-shaped nullcline in a two-variable system [5]. The most common class of ordinary differential equations fulfilling these conditions are two-component systems of the FitzHugh-Nagumo type [6, 7]. The simplest example of such an equation is due to Rinzel and Keller [8]. It is a piecewise linear system with a jump-like discontinuity in one nullcline. The second nullcline is a vertical line. A modified form of this equation (with a non-vertical second nullcline) can be written in the following form [9, 10]:

$$\dot{u} = \mu\,[-u + v - b + \theta(u - d)]\,,$$
$$\dot{v} = -e\,u + v\,. \qquad (1)$$

Figure 1 illustrates the phase plane of (1) with the two nullclines.

Let us first look at the steady state pattern of (1). In general there exist four different possibilities (depending on the three parameters b, d, and e):

(i) One steady state, located on the upper branch of the Z-shaped nullcline, exists if either

$$\text{(case a)} \quad e\,d > b + d \quad \text{and} \quad e > 1, \quad \text{or}$$
$$\text{(case b)} \quad e\,d < d + b - 1 \quad \text{and} \quad e < 1\,.$$

(ii) One steady state, located on the middle (vertical) branch of the first nullcline, exists if

$$b + d > e\,d > d + d - 1 \quad \text{and} \quad e \geqq 1\,.$$

Strictly speaking, this particular "steady state" does not exist since it lies on the discontinuity of one

0340-4811 / 83 / 0600-0648 $ 01.3 0/0. – Please order a reprint rather than making your own copy.

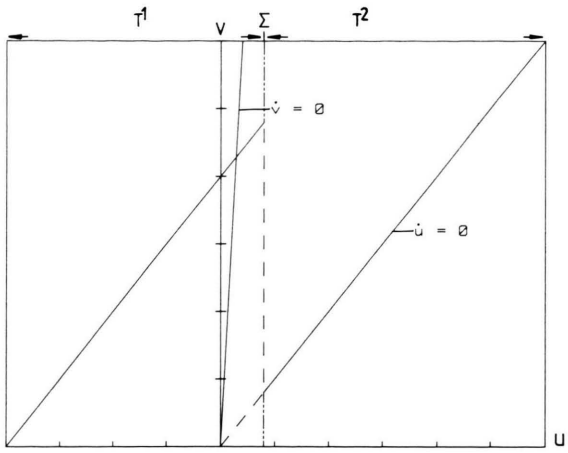

Fig. 1. Nullclines of (1). T^1: left-hand half plane, T^2: right-hand half plane, Σ: dividing line between the two half planes, $\dot{u}=0$: z-shaped nullcline, $\dot{v}=0$: straight nullcline. Parameters: $b=1$, $d=0.2$, $e=15$. Axes: $u=-1.0\ldots 1.5$, $v=0.0\ldots 1.5$.

nullcline; on the other hand, any neighborhood behaves as if it were there, so that it can safely be included.

(iii) One steady state, located on the lower branch, exists if

(case a) $e\,d<b+d-1$ and $e>1$, or

(case b) $e\,d>b+d$ and $e<1$.

(iv) Three steady states coexist for

$$b+d<e\,d<b+d-1 \quad \text{and} \quad e<1\,.$$

Case (i, a) is represented in Figure 1. This is the case to be considered in the following. The steady state has the coordinates

$$\bar{U}=\frac{b}{e-1}\,,$$

$$\bar{V}=\frac{b\,e}{e-1}\,. \tag{2}$$

Aside from this "real steady state" $(\bar{U},\bar{V})$ – which for short may be written $\bar{L}$ where $\bar{L}$ is a vector – there is another, "virtual steady state" $(\tilde{L})$ defined by the intersection of the $\dot{v}=0$ nullcline on the one hand and the (dashed) extension to the left of the lower branch of the Z-shaped nullcline on the other (see Figure 1). This steady state $\tilde{L}$ has the coordinates

$$\tilde{U}=\frac{b-1}{e-1}\,,\qquad \tilde{V}=\frac{e(b-1)}{e-1}\,. \tag{3}$$

Because of the jump discontinuity on the right-hand side of (1) the state plane decomposes naturally into two subsets $u\leqq d$ (in the following termed T^1) and $u\geqq d$ (termed T^2) whereby T^1 and T^2 have only boundary points (the elements of Σ) in common ($\Sigma:=T^1\cap T^2=\bar{T}^1\cap\bar{T}^2$; $\mathring{T}^1\cap\mathring{T}^2=\emptyset$).

The inhomogeneity of (1) can be resolved by transforming to steady state coordinates. For left-hand states (that is, $l\in T^1$ where $l=(u,v)$), the system is written as a homogeneous linear differential equation:

$$\begin{aligned}\dot{u}&=(u-\bar{U})\dot{}=\mu\,[-(u-\bar{U})+(v-\bar{V})]\,,\\ \dot{v}&=(v-\bar{V})\dot{}=-e(u-\bar{U})+(v-\bar{V})\,.\end{aligned} \tag{4}$$

For right-hand states ($l\in T^2$), the system is governed by the virtual steady state $\tilde{L}$. It is now described by the following homogeneous linear differential equation

$$\begin{aligned}\dot{u}&=(u-\tilde{U})\dot{}=\mu\,[-(u-\tilde{U})+(v-\tilde{V})]\,,\\ \dot{v}&=(v-\tilde{V})\dot{}=-e(u-\tilde{U})+(v-\tilde{V})\end{aligned} \tag{5}$$

which differs from (4) only in having the bars replaced by tildes. Note that the virtual steady state $\tilde{L}$, being in T^1, is only a "fata morgana". On trying to approach it (inside T^2), the system will sooner or later enter T^1, meaning that $\tilde{L}$ then has suddenly disappeared while the system finds itself in the region of influence of $\bar{L}$.

By introducing relative coordinates – namely, $\bar{u}:=u-\bar{U}$, $\bar{v}:=v-\bar{V}$, and $\tilde{u}:=u-\tilde{U}$, $\tilde{v}:=v-\tilde{V}$ – and suppressing the bars and the tildes, (4) and (5) are written as

$$\begin{pmatrix}\dot{u}\\ v\end{pmatrix}=\begin{pmatrix}-\mu & \mu\\ -e & 1\end{pmatrix}\begin{pmatrix}u\\ v\end{pmatrix}. \tag{6}$$

This equation can be written more concisely

$$\dot{l}=\mathbb{A}\,l\,, \tag{6a}$$

where $\mathbb{A}$ is the system matrix. Its characteristic equation is

$$\begin{aligned}\lambda^2-\lambda\,\mathrm{tr}\,\mathbb{A}+\det\mathbb{A}&=0\,,\\ \lambda^2+\lambda(\mu-1)+\mu(e-1)&=0\,.\end{aligned} \tag{7}$$

It yields the eigenvalues

$$\lambda_{1/2}=\frac{1-\mu}{2}\pm\sqrt{\left(\frac{\mu+1}{2}\right)^2-e\,\mu}\,. \tag{8}$$

In Fig. 2 the spectrum of matrix $\mathbb{A}$ is plotted as a function of the parameter μ. Figures 2a and 2b

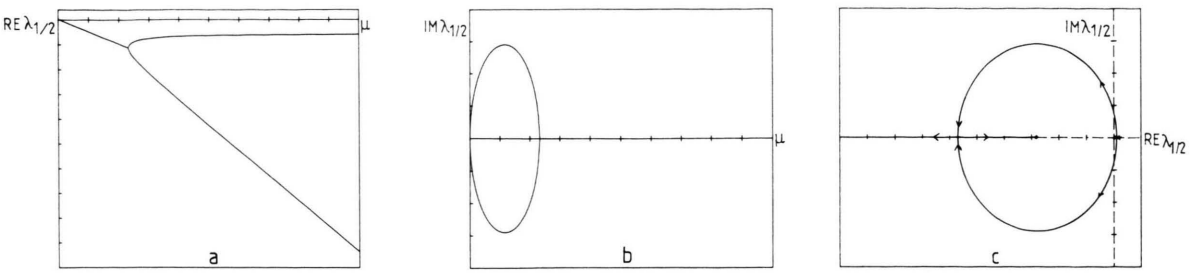

Fig. 2. Eigenvalues of the matrix $\mathbb{A}$ of (6) as a function of μ. (a) real part; (b) imaginary part; (c) real vs. imaginary part, with the arrows indicating the direction of growing μ. *Parameters:* $b = 1$, $d = 0.2$, $e = 15$. *Axes:* a) $\mu = 0 \ldots 250$, $\mathrm{Re}\,\lambda_{1/2} = -250 \ldots 10$; b) $\mu = 0 \ldots 250$, $\mathrm{Im}\,\lambda_{1/2} = -20 \ldots 20$; c) $\mathrm{Re}_{1/2} = -50 \ldots 5$, $\mathrm{Im}\,\lambda_{1/2} = -20 \ldots 20$.

show the real and imaginary part both of λ_1 and λ_2, while Fig. 2c gives a picture of the complex plane, with μ being the curve parameter.

One sees that for $e > 1$ (case i, a above) the system undergoes a bifurcation at $\mu = 1$: A little below this value the steady state is an unstable focus, above it is a stable focus. As μ increases, the two conjugate complex eigenvalues coalesce (at the threshold value $\mu_c = (2e - 1) + 2\sqrt{e(e-1)}$) and become real negative for larger values of μ (Figure 2a, b). If μ is increased even further, the system (1) becomes "stiff" in the sense of numerical mathematics (see, for example, [11]). More specifically, for $\mu \to \infty$ the eigenvalues $\lambda_{1/2}$ tend to $(e - \mu)$ and $(1 - e)$, respectively. This means that the system "relaxes" much faster in the direction of the first eigenvector than in the direction of the second.

The steady state $\bar{L}$ is a global repellor for $\mu < 1$ while for $\mu > \mu_c$ it is a global attractor as is easy to verify. For $\mu \in (1, \mu_c)$, however, the situation is slightly more complicated. In this case $\bar{L}$ (as well as $\tilde{L}$) is a stable focus. Nonetheless, a pair of surrounding limit cycles (one stable and one unstable) of finite amplitude may appear (region LC in Figure 4). This happens, intuitively speaking, when the system, spiralling closer toward $\bar{L}$ ($\in T^1$), thereby transverses the boundary Σ and as a consequence is inside the regime governed by $\tilde{L}$ (that is T^2). It then tries to reach $\tilde{L}$ until it inevitably reenters T^1 – but this time further away from $\bar{L}$ than before. (An analytic description of this behavior will be possible on the basis of the formalism described in Section 6.) Limit cycles here always appear in pairs, with the unstable one separating the attractive regime of the stable focus from that of the stable limit cycle.

Figure 3 illustrates the shape of the stable limit cycle for several different values of μ. The smaller

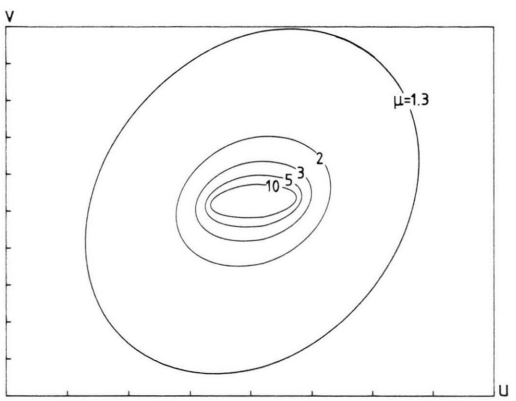

Fig. 3. Limit cycle solutions of (1) for different values of μ as indicated. Numerical simulation using a standard Runge-Kutta-Merson integration routine. *Parameters:* $b = 1$, $d = 0.2$, $e = 15$. *Axes:* $u = -4 \ldots 4$, $v = -10 \ldots 10$.

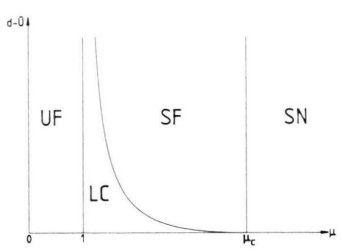

Fig. 4. Schematic representation of the bifurcation plane of (1). UF: region of unstable focus or node; LC: region of limit cycles and stable focus coexisting; SF: region of stable focus; SN: region of stable node.

(and less circular) limit cycles correspond to larger values of μ.

Figure 4 gives an overview of the qualitative behavior of (1). The ordinate $(d - \bar{U})$ is the distance between the threshold d and the steady state value $\bar{U}$. The abscissa is the stiffness (or damping) parameter μ. One sees that for $(d - \bar{U})$ sufficiently small,

even relatively large values of $\mu (< \mu_c)$ still give limit cycles.

After having considered the qualitative behavior in dependence on the eigenvalues, let us now consider the eigenvectors explicitly. The normalized eigenvectors of the matrix $\mathbb{A}$ are

$$y^i = \left[\left(\frac{\mu}{\mu + \lambda_i} \right)^2 + 1 \right]^{-1/2} \begin{pmatrix} \frac{\mu}{\mu + \lambda_i} \\ 1 \end{pmatrix} \tag{9}$$

where $i = 1, 2$.

One sees that for $\mu \gg 1$ the first ("fast") eigenvector has hardly any v-component at all (its u-component is approximately μ/e times its v-component) while the second ("slow") eigenvector points almost in the direction of the stable branch of the Z-shaped nullcline.

Let us proceed to the behavior of the whole system, Fig. 5 shows that two types of excitable behavior can be distinguished, one bound on a stable focus (Fig. 5a), and one bound on a stable node (Fig. 5b). In either case, an initial condition close to the stable steady state returns to the latter on a "round-about" course (cf. [6] and [9]).

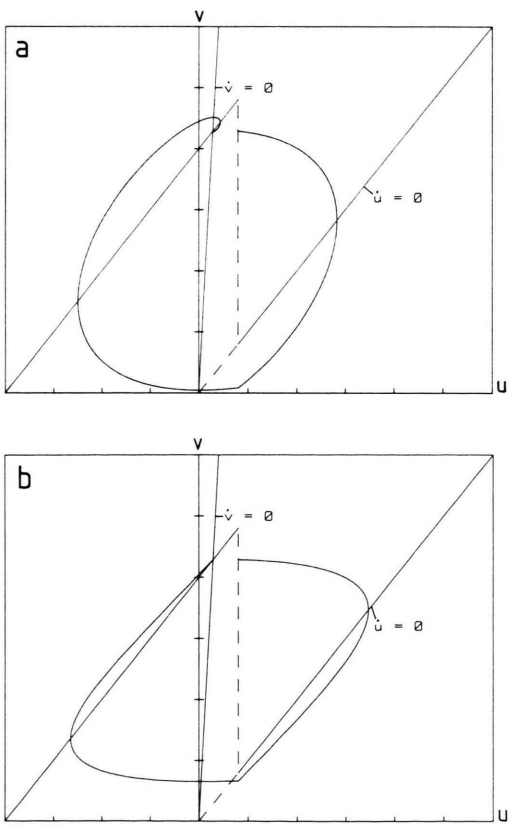

Fig. 5. Super-threshold excitation of the system of (1) for (a) $\mu = 28$ ($< \mu_c$) and (b) $\mu = 100$ ($> \mu_c$). *Other parameters:* $b = 1$, $d = 0.2$, $e = 15$. *Axes:* $u = -1.0 \ldots 1.5$, $v = 0.0 \ldots 1.5$.

3. The Diffusion-Coupled System

Whenever there is a spatial coupling present (in the first component, at least) one obtains for the whole system a parabolic partial differential equation:

$$\begin{aligned} \partial_t u &= \mathbb{D}_{uu} \partial_r^2 u + \mu [-u + v - b + \theta(u - d)], \\ \partial_t v &= \qquad\quad -e u \quad + v . \end{aligned} \tag{10}$$

The diffusion matrix is very simple (containing just one entry, $\mathbb{D}_{uu}$). By an appropriate spatial stretching (transformation of the length by a factor of $1/\sqrt{\mathbb{D}_{uu}}$), this matrix is changed into $\begin{pmatrix} 1 & 0 \\ 0 & 0 \end{pmatrix}$. As we are only interested in wavetrains of constant shape, we may now introduce a "wave variable"

$$\xi := r - c t \tag{11}$$

where c is the wave velocity.

Space-time now reduces to one-dimensional ξ-space. At the same time, Eq. (10) transforms into the ordinary differential equation

$$\begin{aligned} -c u' &= u'' + \mu [-u + v - b + \theta(u - d)], \\ -c v' &= \quad -e u \quad + v , \end{aligned} \tag{12}$$

where the prime corresponds to $\mathrm{d}/\mathrm{d}\xi$.

Introduction of the new variable w ($w := u'$) transforms the second-order system (12) into the three-dimensional first-order system

$$\begin{aligned} u' &= w , \\ v' &= (1/c)\,(e u - v) \\ w' &= \mu [u - v + b - \theta(u - d)] - c w . \end{aligned} \tag{13}$$

The spatially homogeneous steady states of this system are the same as those of the local system, that is,

$$\bar{U} = \frac{b}{e - 1}, \quad \bar{V} = \frac{b e}{e - 1}, \quad \bar{W} = 0 ,$$

and

$$\tilde{U} = \frac{b - 1}{e - 1}, \quad \tilde{V} = \frac{e(b - 1)}{e - 1}, \quad \tilde{W} = 0 , \tag{14}$$

respectively.

Here again, $\bar{L}$ is the real and $\tilde{L}$ the virtual steady state; also, T^1 and T^2 are defined just as in the local case, namely,

$$T^1 := \{l : u \leqq d\}; \quad T^2 := \{l : u \geqq d\}. \tag{15}$$

Transforming (13) in such a way that a steady state becomes the origin (cf. the procedure leading to (6)) yields

$$\begin{pmatrix} u \\ v \\ w \end{pmatrix}' = \begin{pmatrix} 0 & 0 & 1 \\ e/c & -1/c & 0 \\ \mu & -\mu & c \end{pmatrix} \begin{pmatrix} u \\ v \\ w \end{pmatrix} \tag{16}$$

or, equivalently,

$$l' = \mathbb{B}\, l. \tag{16a}$$

This is our final equation. Note that it applies twice, so to speak, once for each of the two regions (T^1 and T^2) that are both described by this equation.

4. Linear Analysis

The eigenvalues of λ_i of the matrix $\mathbb{B}$ (in (16a)) are the roots of

$$\lambda^3 - \lambda^2 \operatorname{tr} \mathbb{B} + \lambda \min \mathbb{B} - \det \mathbb{B} = 0, \tag{17}$$

where

$$\operatorname{tr} \mathbb{B} = -\frac{c^2 - 1}{c},$$

$$\min \mathbb{B} = 1 - \mu,$$

$$\det \mathbb{B} = \frac{\mu}{c}(e - 1).$$

These roots can be found using Cardano's formula. Figure 6 summarizes the results obtained.

One sees that one eigenvalue is always real negative while the two others (being either complex-conjugate or real) always have a positive real part. Correspondingly, the steady states of (13) are of the saddle-focus or the saddle-node type, respectively. There is no stable steady state possible.

Because of the instability of all solutions of the linear system (16), any attempt at calculating the constant shape wave solutions of the original partial differential equation (10), via (16), directly by a local numerical integration routine (like that of Runge and Kutta, cf. [12]) is doomed to fail because the result necessarily diverges (at least because of numerical errors), and so in both time directions. This "saddle character" appears to be a general feature of constant shape wave solutions of reaction diffusion equations. In consequence, "non-local methods" that from the beginning take into explicit account the boundary conditions, have to be used (see next Section).

The normalized eigenvectors of matrix $\mathbb{B}$ (16a) are

$$t^i = \frac{1}{N_i} \begin{pmatrix} 1 \\ \dfrac{e}{1 + \lambda_i c} \\ \lambda_i \end{pmatrix} \tag{18}$$

with normalisation factor

$$N_i = \left(\frac{|1 + \lambda_i c|^2 (1 + |\lambda_i|^2) + e^2}{|1 + \lambda_i c|^2} \right)^{1/2}$$

where $i = 1, 2, 3$.

The three eigenvectors taken together form the transformation matrix

$$\mathbb{H} := (t^1, t^2, t^3). \tag{19}$$

It transforms the complex x, y, z-space (k-space) spanned by the complex eigenvectors into the real u, v, w-space (l-space). Specifically,

$$l = \mathbb{H}\, k. \tag{20}$$

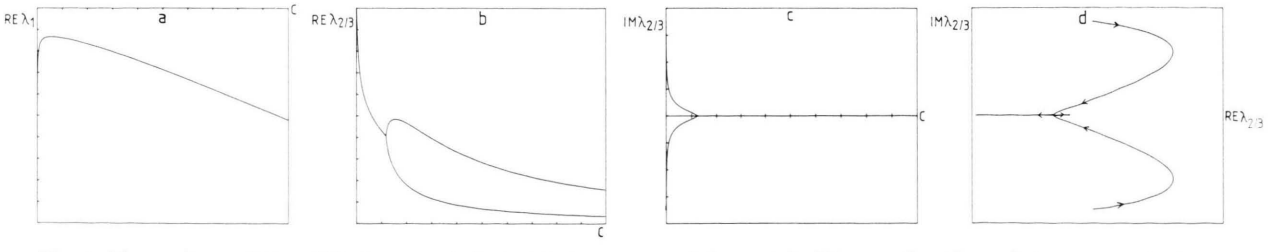

Fig. 6. Eigenvalues of the diffusion coupled system (spectrum of the matrix $\mathbb{B}$) as a function of the wave-velocity c. Compare Figure 2. *Parameters:* $b = 1$, $d = 0.2$, $e = 15$, $\mu = 100$. *Axes:* a) $c = 0 \ldots 50$, $\lambda_1 = -100 \ldots 0$; b) $c = 0 \ldots 50$, Re $\lambda_{2/3} = 0 \ldots 10$; c) $c = 0 \ldots 50$, Im $\lambda_{2/3} = -40 \ldots 40$; d) Re $\lambda_{2/3} = 0 \ldots 10$, Im $\lambda_{2/3} = -40 \ldots 40$.

$\mathbb{H}$, the matrix of eigenvectors, diagonalizes the system matrix $\mathbb{B}$, yielding

$$\mathbb{H}^{-1}\,\mathbb{B}\,\mathbb{H}=\begin{pmatrix}\lambda_1 & 0 & 0\\ 0 & \lambda_2 & 0\\ 0 & 0 & \lambda_3\end{pmatrix}. \tag{21}$$

The steady states behave under the transformation $\mathbb{H}$ like vectors:

$$L=\mathbb{H}K. \tag{20a}$$

The jump condition (see (13)) takes the following form in k-space:

$$\mathbb{H}_{11}x+\mathbb{H}_{12}y+\mathbb{H}_{13}z=d. \tag{22}$$

That is, the formerly vertical threshold plane (defined by $u=d$) is now replaced by a slanted plane, defined by (22). The whole original equation (13) becomes in the new coordinates

$$\begin{pmatrix}x\\ y\\ z\end{pmatrix}'=\begin{pmatrix}\lambda_1 & 0 & 0\\ 0 & \lambda_2 & 0\\ 0 & 0 & \lambda_3\end{pmatrix}\begin{pmatrix}x\\ y\\ z\end{pmatrix}+\mathbb{H}^{-1}\begin{pmatrix}0\\ 0\\ b-\theta(\mathbb{H}_{11}x+\mathbb{H}_{12}y+\mathbb{H}_{13}z-d)\end{pmatrix}. \tag{23}$$

The solution of (23) becomes, with initial condition $(\alpha+\bar{X},\beta+\bar{Y},\gamma+\bar{Z})\in T^1$ at $\xi=\xi_0$:

$$\begin{pmatrix}x(\xi)\\ y(\xi)\\ z(\xi)\end{pmatrix}=\begin{pmatrix}\alpha\\ 0\\ 0\end{pmatrix}e^{\lambda_1(\xi-\xi_0)}+\begin{pmatrix}0\\ \beta\\ 0\end{pmatrix}e^{\lambda_2(\xi-\xi_0)}+\begin{pmatrix}0\\ 0\\ \gamma\end{pmatrix}e^{\lambda_3(\xi-\xi_0)}+\begin{pmatrix}\bar{X}\\ \bar{Y}\\ \bar{Z}\end{pmatrix}. \tag{24}$$

In the other half-space T^2, the same equation applies, except that the bar becomes a tilde and that the initial condition is now from T^2, that is $(\alpha+\tilde{X},\beta+\tilde{Y},\gamma+\tilde{Z})\in T^2$.

With (24) given, we now know explicitly the trajectories determined by an arbitrary initial condition located either in T^1 or T^2. Our next task is to describe explicitly also the "composed" trajectories that cross the boundary (Σ) between the two half-spaces. To do this it is necessary to determine the location of the "crossing points" in ξ-space.

5. Finite Wavetrains on the Infinite Linear Fiber

The results of the preceding Section can now be used to solve the boundary value problem for the linear fiber. We suppose natural (Dirichlet-type) boundary conditions, that is, boundary conditions kept fixed at the steady state value $\bar{K}$ at infinity ($\xi=\pm\infty$).

Figure 7 schematically shows a wavetrain of N pulses travelling from left to right on the infinite fiber. One sees that for sufficiently large negative values of the wave variable ξ, the solution forever remains within the left-hand half-plane of the two-dimensional phase space of the local system. For $\xi\to-\infty$, the solution is therefore described by

$$\begin{pmatrix}x(\xi)\\ y(\xi)\\ z(\xi)\end{pmatrix}=\begin{pmatrix}0\\ \beta_1\\ 0\end{pmatrix}e^{\lambda_2(\xi-\xi_0)}+\begin{pmatrix}0\\ 0\\ \gamma_1\end{pmatrix}e^{\lambda_3(\xi-\xi_0)}+\begin{pmatrix}\bar{X}\\ \bar{Y}\\ \bar{Z}\end{pmatrix}. \tag{25}$$

The same reasoning applies to the outermost right-hand portion of the wavetrain ($\xi\to+\infty$), yielding

$$\begin{pmatrix}x(\xi)\\ y(\xi)\\ z(\xi)\end{pmatrix}=\begin{pmatrix}\alpha_1\\ 0\\ 0\end{pmatrix}e^{\lambda_1(\xi-\xi_0)}+\begin{pmatrix}\bar{X}\\ \bar{Y}\\ \bar{Z}\end{pmatrix}. \tag{26}$$

Both equations contain the boundary condition ($\bar{K}$). The values that already apply at infinity (namely, those of the local steady state $\bar{K}$) are at large (positive and negative) ξ-values being approached in accordance with the dynamics of the local system. Since the local dynamics is stable (see Sect. 2), this amounts to the constraint that all the potentially divergent terms of (24) have to disappear when the boundary conditions are to be fulfilled. The amplitudes of these terms must therefore be set equal to zero. Setting $\alpha=0$ in (24) indeed leads to (25), and setting both β and γ equal to zero in (24) leads to (26).

Our next aim is to calculate the transition points on the linear fiber (named φ_i in Figure 7). These are the points at which the jump condition (22) is fulfilled. Without loss of generality we can put

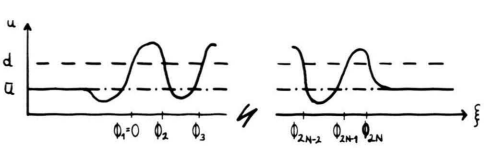

Fig. 7. Schematic representation of a wavetrain containing N pulses on a linear fiber (cf. text).

$\varphi_1 := 0$. Hence in (25) ξ_0 becomes equal to zero. We now choose intervals in ξ-space such that the trajectory remains within the same half-plane of the local state space in each interval. We then in each case take the left-hand boundary value of the interval in question as the origin of ξ-space (since we are free to choose the origin in (24)). This implies $\xi_0 = 0$ in (26). The wave solution in the whole interval $(0, \varphi_i)$ is therefore described by

$$\begin{pmatrix} x(\xi) \\ y(\xi) \\ z(\xi) \end{pmatrix} = \begin{pmatrix} \alpha_i \\ 0 \\ 0 \end{pmatrix} e^{\lambda_1 \xi} + \begin{pmatrix} 0 \\ \beta_i \\ 0 \end{pmatrix} e^{\lambda_2 \xi} + \begin{pmatrix} 0 \\ 0 \\ \gamma_i \end{pmatrix} e^{\lambda_3 \xi} + \hat{K}, \quad (27)$$

where $\hat{K} = \bar{K}$ for odd i and $\hat{K} = \tilde{K}$ otherwise. The amplitudes α_i, β_i, and γ_i are given by

$$\begin{aligned} \alpha_i &= x(\varphi_{i-1}) - \hat{X}, \\ \beta_i &= y(\varphi_{i-1}) - \hat{Y}, \\ \gamma_i &= z(\varphi_{i-1}) - \hat{Z}, \end{aligned} \quad (28)$$

where $\hat{X}$, $\hat{Y}$, $\hat{Z}$ are components of the vector $\hat{K}$.

Using these formulas, we now obtain the jump condition at the left boundary of the first, then of the second interval, and so forth. Labeling the jump conditions successively as (1), (2), etc. we have

$$\begin{aligned}
&(1) && \text{for } \xi = \varphi_1 = 0: \\
&&& \mathbb{H}_{11}\bar{X} + \mathbb{H}_{12}(\beta_1 + \bar{Y}) + \mathbb{H}_{13}(\gamma_1 + \bar{Z}) = d, \\
&&& \text{that is:} \\
&&& \mathbb{H}_{12}\beta_1 + \mathbb{H}_{13}\gamma_1 + \bar{U} = d; \\
&(2) && \text{for } \xi = \varphi_2: \\
&&& \mathbb{H}_{11}\alpha_3 + \mathbb{H}_{12}\beta_3 + \mathbb{H}_{13}\gamma_3 + \bar{U} = d; \\
&(3) && \text{for } \xi = \varphi_3: \\
&&& \mathbb{H}_{11}\alpha_4 + \mathbb{H}_{12}\beta_4 + \mathbb{H}_{13}\gamma_4 + \tilde{U} = d; \\
&&& \vdots \qquad\qquad \vdots \qquad\qquad (29) \\
&(2i-1) && \text{for } \xi = \varphi_{2i-1}: \\
&&& \mathbb{H}_{11}\alpha_{2i} + \mathbb{H}_{12}\beta_{2i} + \mathbb{H}_{13}\gamma_{2i} + \tilde{U} = d; \\
&(2i) && \text{for } \xi = \varphi_{2i}: \\
&&& \mathbb{H}_{11}\alpha_{2i+1} + \mathbb{H}_{12}\beta_{2i+1} + \mathbb{H}_{13}\gamma_{2i+1} + \bar{U} = d; \\
&&& \vdots \qquad\qquad \vdots \\
&(2N) && \text{for } \xi = \varphi_{2N}: \\
&&& \mathbb{H}_{11}\alpha_1 + \bar{U} = d.
\end{aligned}$$

The whole system of equations (29) contains $2N$ equations in $6N$ unknowns (namely, the $2N$ triples α_i, β_i, γ_i). In addition, there are $(2N-1)$ further unknowns present in (29), namely, all of the φ_i (except the first, φ_1, which could be choosen freely).

Aside from the jump conditions, the wave solutions have also to fulfill "matching conditions", since continuity at the φ_i-values is required (see (28)). These conditions can be specified by writing (24) down for every boundary between two intervals. This yields

$$\begin{aligned}
&(1) && \text{for } \xi = \varphi_1 = 0: \\
&&& \text{(a)} \quad \bar{X} = \alpha_2 + \tilde{X}, \\
&&& \text{(b)} \quad \beta_1 + \bar{Y} = \beta_2 + \tilde{Y}, \\
&&& \text{(c)} \quad \gamma_1 + \bar{Z} = \gamma_2 + \tilde{Z}; \\
&(2) && \text{for } \xi = \varphi_2: \\
&&& \text{(a)} \quad \alpha_2 e^{\lambda_1\varphi_2} + \tilde{X} = \alpha_3 + \bar{X}, \\
&&& \text{(b)} \quad \beta_2 e^{\lambda_2\varphi_2} + \tilde{Y} = \beta_3 + \bar{Y}, \\
&&& \text{(c)} \quad \gamma_2 e^{\lambda_3\varphi_2} + \tilde{Z} = \gamma_3 + \bar{Z}; \\
&&& \vdots \qquad\qquad \vdots \\
&(2i-1) && \text{for } \xi = \varphi_{2i-1}: \\
&&& \text{(a)} \quad \alpha_{2i-1} e^{\lambda_1\varphi_{2i-1}} + \bar{X} = \alpha_{2i} + \tilde{X}, \\
&&& \text{(b)} \quad \beta_{2i-1} e^{\lambda_2\varphi_{2i-1}} + \bar{Y} = \beta_{2i} + \tilde{Y}, \qquad (30) \\
&&& \text{(c)} \quad \gamma_{2i-1} e^{\lambda_3\varphi_{2i-1}} + \bar{Z} = \gamma_{2i} + \tilde{Z}; \\
&(2i) && \text{for } \xi = \varphi_{2i}: \\
&&& \text{(a)} \quad \alpha_{2i} e^{\lambda_1\varphi_{2i}} + \tilde{X} = \alpha_{2i+1} + \bar{X}, \\
&&& \text{(b)} \quad \beta_{2i} e^{\lambda_2\varphi_{2i}} + \tilde{Y} = \beta_{2i+1} + \bar{Y}, \\
&&& \text{(c)} \quad \gamma_{2i} e^{\lambda_3\varphi_{2i}} + \tilde{Z} = \gamma_{2i+1} + \bar{Z}; \\
&&& \vdots \qquad\qquad \vdots \\
&(2N) && \text{for } \xi = \varphi_{2N}: \\
&&& \text{(a)} \quad \alpha_{2N} e^{\lambda_1\varphi_{2N}} + \tilde{X} = \alpha_1 + \bar{X}, \\
&&& \text{(b)} \quad \beta_{2N} e^{\lambda_2\varphi_{2N}} + \tilde{Y} = \bar{Y}, \\
&&& \text{(c)} \quad \gamma_{2N} e^{\lambda_3\varphi_{2N}} + \tilde{Z} = \bar{Z}.
\end{aligned}$$

This chain-like system (30) can be decomposed into three subsystems because the α's, β's, and γ's are completely decoupled from each other. Looking first at the α's, one sees that the first line (1 a) of (30) can be solved for α_2; using this result, the fourth line (2 a) yields α_3 (as a function of α_2), and so forth. Thus, there is a finite recursion which gives us every α_i as an explicit function of the preceding one. To repeat:

$$\begin{aligned} \alpha_2 &= \bar{X} - \tilde{X}, \\ \alpha_3 &= (\bar{X} - \tilde{X})(e^{\lambda_1\varphi_2} - 1), \\ &\vdots \end{aligned} \quad (31)$$

or, written more concisely,

$$\alpha_i = (\bar{X} - \tilde{X}) \left(\sum_{k=2}^{i-1} (-1)^k \exp\left(\lambda_1 \sum_{l=k}^{i-1} \varphi_l \right) + (-1)^i \right) \quad (32)$$

where $i = 2, \ldots, 2N$.

The general formula is (32). Remains the crowning final step of the recursion. For α_1 – which appears in the last block of (30) – we obtain

$$\alpha_1 = (\bar{X} - \tilde{X}) \left(\sum_{k=2}^{2N} (-1)^k \exp\left(\lambda_1 \sum_{l=k}^{2N} \varphi_l \right) - 1 \right). \quad (33)$$

We therefore have obtained explicit expressions for all of the α_i.

Proceeding to the β's, we start with the last but one line ($2N\,b$) of (30). Using it, we find, in analogy to (31),

$$\begin{aligned} \beta_{2N} &= (\bar{Y} - \tilde{Y})\, e^{-\lambda_2 \varphi_{2N}}, \\ \beta_{2N-1} &= (\bar{Y} - \tilde{Y})\, (e^{-\lambda_2(\varphi_{2N} + \varphi_{2N-1})} - e^{-\lambda_2 \varphi_{2N-1}}), \quad (34) \\ &\vdots \end{aligned}$$

This time we have a recursion that runs backwards, so to speak. The intermediate steps are, in analogy to (32),

$$\beta_{2N-i} = (\bar{Y} - \tilde{Y}) \sum_{k=2N-i}^{2N} (-1)^k \exp\left(-\lambda_2 \sum_{l=2N-i}^{k} \varphi_l \right) \quad (35)$$

In the final step we arrive at β_1, obtaining, in analogy to (33),

$$\beta_1 = (\bar{Y} - \tilde{Y}) \left(\sum_{k=2}^{2N} (-1)^k \exp\left(-\lambda_2 \sum_{l=2}^{k} \varphi_l \right) - 1 \right). \quad (36)$$

The γ's are again found analogously, by substituting γ_i for β_i, λ_3 for λ_2, $\bar{Z}$ for $\bar{Y}$, and $\tilde{Z}$ for $\tilde{Y}$, respectively, in (34–36).

Thus, we have, using the results of (30), obtained all the amplitudes (α_i, β_i, γ_i) as functions of both the interval lengths φ_i and (via the λ_i and $\mathbb{H}_{ij}$, which are functions of c) the wave velocity c.

If we now insert these amplitudes (31–36) into (29), we obtain a system of nonlinear algebraic equations that contains only the wave variables φ_i as well as c as the unknowns. This implicit equation is a *dispersion relation* since it connects wave properties (wavelength, velocity, etc.) with medium properties (excitability, local dynamics parameters, etc.).

This dispersion relation contains all information about all wave solutions on the linear fiber. Before going to extract this information from the dispersion relation, we still have one minor point to consider. As the first of the φ_i (namely φ_1) is already known, we obtain $2N$ equations not in $2N+1$ variables, but rather in $2N$ variables (namely, c, $\varphi_2, \ldots, \varphi_{2N}$). Such algebraic systems have, if they possess any solution at all, only solutions of dimension zero (that is, points) that are locally unique. This follows from the implicit function theorem (cf. e.g. [13]). Therefore, the linear fiber (unlike the ring fiber to be discussed later) cannot be "tuned through" continuously in c. Rather, there is a discrete spectrum of solutions in c,φ-space. In other words, the solutions of (29) are isolated points in c,φ-space rather than curves.

As a side remark, it may be noted that it is possible to subject the linear fiber to an "external tuning through". If we introduce the threshold parameter $(d - \bar{U})$ as a tunable external parameter, we can obtain a continuous connection between wave propagation velocity (c) on the one hand, and the excitation properties of the medium on the other. A special relation of this type (namely, between wave propagation velocity on the one hand, and a property of the medium – like its complex dielectricity constant – on the other) is knwon in classical electrodynamics under the name of Kramers-Kronig dispersion relation (see e.g. [14]). We therefore have found a (formally different) analogue in a reaction-diffusion system.

6. Finite Wavetrains on the Ring Fiber

Circular fibers are at least as important as the linear ones. On the one hand, the linear fiber is (in a certain sense) equivalent to a ring of infinite length. On the other hand, the ring lends itself to more applications. Coupled concentric rings, for example, provide a starting point for considering two-dimensional media (cf. [2]).

Most of the above procedures carry over. Let φ_i again denote the length of the i-th interval; cf. Figure 8.

As the system is cyclic, $\varphi_{2N+1} = \varphi_1$. We can therefore define a cyclic group, $I := (\{0, 1, \ldots, 2N\}, +)$, where "+" refers to composition. The dynamics on the ring are invariant under transformations gen-

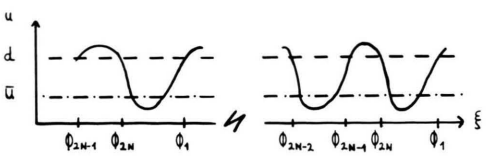

Fig. 8. Schematic representation of a wavetrain containing N pulses on a ring fiber (cf. Figure 7).

erated by I_e, where I_e refers to the subgroup of the even (I_e) integers in I.

When we choose $\eta^i := (\eta_1^i, \eta_2^i, \eta_3^i) := (\alpha_i, \beta_i, \gamma_i)$, for the amplitudes, the jump conditions on the ring become (compare (29)):

$$\begin{aligned}
&(1) \quad \text{for } \xi = \varphi_1: && \sum_{j=1}^{3} \mathbb{H}_{1j}\, \eta_j^2 && + \tilde{U} = d\,,\\
&(2) \quad \text{for } \xi = \varphi_2: && \sum_{j=1}^{3} \mathbb{H}_{1j}\, \eta_j^3 && + \bar{U} = d\,,\\
&\quad\vdots && \vdots && \\
&(2i-1) \quad \text{for } \xi = \varphi_{2i-1}: && \sum_{j=1}^{3} \mathbb{H}_{1j}\, \eta_j^{2i} && + \tilde{U} = d\,, \qquad (37)\\
&(2i) \quad \text{for } \xi = \varphi_{2i}: && \sum_{j=1}^{3} \mathbb{H}_{1j}\, \eta_j^{2i+1} && + \bar{U} = d\,,\\
&\quad\vdots && \vdots && \\
&(2N) \quad \text{for } \xi = \varphi_{2N}: && \sum_{j=1}^{3} \mathbb{H}_{1j}\, \eta_j^{1} && + \bar{U} = d\,.
\end{aligned}$$

Once again, there are $2N$ equations in $6N$ unknowns. The continuity conditions (cf. (30)) now read

$$\begin{aligned}
&(1) \quad \text{for } \xi = \varphi_1:\\
&\qquad \eta_j^1 \quad e^{\lambda_j \varphi_1} && + \bar{K}_j = \eta_j^2 && + \tilde{K}_j\,,\\
&(2) \quad \text{for } \xi = \varphi_2:\\
&\qquad \eta_j^2 \quad e^{\lambda_j \varphi_2} && + \tilde{K}_j = \eta_j^3 && + \bar{K}_j\,,\\
&\qquad\vdots && \vdots && \\
&(2i-1) \quad \text{for } \xi = \varphi_{2i-1}:\\
&\qquad \eta_j^{2i-1}\, e^{\lambda_j \varphi_{2i-1}} && + \bar{K}_j = \eta_j^{2i} && + \tilde{K}_j\,, \qquad (38)\\
&(2i) \quad \text{for } \xi = \varphi_{2i}:\\
&\qquad \eta_j^{2i} \quad e^{\lambda_j \varphi_{2i}} && + \tilde{K}_j = \eta_j^{2i+1} && + \bar{K}_j\,,\\
&\qquad\vdots && \vdots && \\
&(2N) \quad \text{for } \xi = \varphi_{2N}:\\
&\qquad \eta_j^{2N} \quad e^{\lambda_j \varphi_{2N}} && + \tilde{K}_j = \eta_j^{1} && + \bar{K}_j\,,
\end{aligned}$$

with $j = 1, 2, 3$.

This system of $2N$ equations is cyclic by virtue of the symmetry of the problem. Therefore there does not exist any special amplitude vector this time that could be solved for directly. The solution must instead be found by working through the whole recursion.

Without loss of generality we may start out at φ_1, to then obtain the next amplitude directly (from (38))

$$\eta_j^2 = \eta_j^1\, e^{\lambda_j \varphi_1} + (\bar{K}_j - \tilde{K}_j)\,. \qquad (39)$$

Comparing (39) with (31), one sees that the first term is new while the second is familiar. (As for the α's this second term is the same as before, but the β's and γ's are now all generated in perfect analogy to the α's.) Specifically, we have for a general η^i

$$\begin{aligned}
\eta_j^i = \eta_j^1 \exp\left(\lambda_j \sum_{l=1}^{i-1} \varphi_l\right) \qquad (40)\\
+ (\bar{K}_j - \tilde{K}_j) \cdot \left(\sum_{k=2}^{i-1} (-1)^k \exp\left(\lambda_j \sum_{l=k}^{i-1} \varphi_l\right) + (-1)^i\right),
\end{aligned}$$

where $j = 1, 2, 3$, while $i = 2, \ldots, 2N$.

Working through all of the η^i, we eventually arrive again at η^1:

$$\begin{aligned}
\eta_j^1 = \eta_j^1 \exp\left(\lambda_j \sum_{l=1}^{2N} \varphi_l\right) \qquad (41)\\
+ (\bar{K}_j - \tilde{K}_j) \cdot \left(\sum_{k=2}^{2N} (-1)^k \exp\left(\lambda_j \sum_{l=k}^{2N} \varphi_l\right) - 1\right).
\end{aligned}$$

This equation can now be solved for η^1:

$$\eta_j^1 = (\bar{K}_j - \tilde{K}_j) \frac{\sum_{k=2}^{2N} (-1)^k \exp\left(\lambda_j \sum_{l=k}^{2N} \varphi_l\right) - 1}{1 - \exp\left(\lambda_j \sum_{l=1}^{2N} \varphi_l\right)}. \qquad (42)$$

Using η^1, it is easy to obtain η^2, then η^3 from η^2, and so forth.

As our starting with φ_1 had been arbitrary, (42) may be generalized toward

$$\eta_j^m = (-1)^m (\bar{K}_j - \tilde{K}_j) \frac{\sum_{k=m+1}^{m-1} (-1)^k \exp\left(\lambda_j \sum_{l=k}^{m-1} \varphi_l\right) - 1}{\exp\left(\lambda_j \sum_{l=1}^{2N} \varphi_l\right) - 1} \qquad (43)$$

whereby it is assumed that we started from an arbitrary η^m rather than from η^1. Equation (43) shows the rotational symmetry of the problem: the indices can safely be shifted. Note that $\sum$ indicates a cyclic summation over all the $2N$ nonzero elements of the group I.

All of the η^i are now given as functions of the φ_i and c. Inserting the η^i (obtained recursively from (40) and (42)) into the jump conditions (37), we obtain $2N$ equations in $2N+1$ unknowns (namely, $c, \varphi_1, \ldots, \varphi_{2N}$). These equations, as long as fulfilling the prerequisites of the implicit function theorem (Jacobian determinant nonzero), define at least locally a one-dimensional manifold in $\mathbb{R}^{2N+1}$. That

is, they define a true dispersion relation in the classical sense because the manifold connects wave velocity and ring length Φ (equal to $\sum_i \varphi_i$).

In other words, by inserting the amplitudes (40) into (37), an implicit analytical expression of the desired dispersion relation has been found. This implicit equation is too long to be repeated here, but it can easily be put into a computer. It will be used for obtaining the computer-generated results of Sections 8–10.

7. Relationships Between Linear Fiber and Ring Fiber

The $2N$ jump conditions ((29) for the linear and (37) for the cyclic fiber, respectively) in each case yield a high-dimensional system of coupled nonlinear algebraic equations. Their solution is a purely technical problem that can be relegated to a computer (see Sections 8–10). Before giving the concrete results, it is worthwhile to briefly discuss the relationships that exist between the general properties of the solutions of the linear and the ring fiber, respectively.

The linear fiber always shows a characteristic asymmetry of the three pulse amplitudes (α_i, β_i, γ_i). This reflects the sign pattern of the eigenvalues (cf. Fig. 6 above). A second remarkable property of the linear fiber is the discreteness of the wave velocity spectrum (shown in Sect. 5; cf. also [15]). To see the situation on the ring, recall that intuitively speaking, a wavetrain on the ring is always subject to a certain amount of "self-interaction" that is decreasing as circumference increases. On the linear fiber, in contrast, a single pulse always runs into a "steady state region" (being the case with the assumed boundary conditions).

If ring length is allowed to go to infinity ($\Phi \to \infty$), the amplitude equation for the first component (η_1^1 or α_1) on the ring, (42), transforms into that for the linear fiber, (33), since $\lim_{\Phi \to \infty} \exp(\lambda_1 \cdot \Phi) = 0$. For the equations for the β's and γ's, this is not the case, however. Since both β_1 and γ_1 on the linear fiber are defined on the right-hand boundary of the interval $(-\infty, 0]$, the limit has to be taken in the direction of negative ξ-values. Substituting $-\lambda_{2/3}$ for $\lambda_{2/3}$ into the equation for the ring (42), we thus indeed once more obtain the equation for the linear fiber (36) as $\Phi \to \infty$.

This shows to two things: (a) The linear fiber is equivalent to a ring of infinite size. (b) The discreteness of the wave velocity in the case of the linear fiber stems from the presence of an additional condition (namely, $\Phi = \infty$) or, differently speaking, from the loss of one variable (φ_1) during the transition from the ring to the linear fiber.

8. Single Pulse on the Linear Fiber

The simplest special case, that of a single pulse on the linear fiber, can be treated one further step analytically. For the linear fiber, the jump and matching conditions (29) and (30) in the first component read

$$\mathbb{H}_{11}\,\alpha_1 = d - \bar{U} \tag{44}$$

and

$$\alpha_1 = (\bar{X} - \tilde{X})\,(e^{\lambda_1 \varphi_2} - 1)\,, \tag{45}$$

respectively, so that

$$\varphi_2 = \frac{1}{\lambda_1} \log\left[\frac{d - \bar{U}}{\mathbb{H}_{11}(\bar{X} - \tilde{X})} + 1\right]. \tag{46}$$

(46) is an explicit expression for the length of the second interval (during which the system is in the super-threshold half-space T^2). Here φ_2 is expressed as a function of c and d. Such an explicit expression can be obtained only in the present special case.

The other amplitudes β_1 and γ_1 can be found similarly to α_1, using (34). This yields

$$\begin{aligned} \beta_1 &= (\bar{Y} - \tilde{Y})\,(e^{-\lambda_2 \varphi_2} - 1)\,, \\ \gamma_1 &= (\bar{Z} - \tilde{Z})\,(e^{-\lambda_3 \varphi_2} - 1\,. \end{aligned} \tag{47}$$

Inserting these amplitudes and φ_2 (from (46)) into the first line of (29), we obtain

$$\mathbb{H}_{12}(\bar{Y} - \tilde{Y})\left[\left(\frac{d - \bar{U}}{\mathbb{H}_{11}(\bar{X} - \tilde{X})} + 1\right)^{-\lambda_2/\lambda_1} - 1\right] + \tag{48}$$

$$\mathbb{H}_{13}(\bar{Z} - \tilde{Z})\left[\left(\frac{d - \bar{U}}{\mathbb{H}_{11}(\bar{X} - \tilde{X})} + 1\right)^{-\lambda_3/\lambda_1} - 1\right] + \bar{U} = d\,.$$

This implicit equation defines a one-dimensional manifold in c,d-space (because the λ_i and $\mathbb{H}_{ij}$ are functions of c), showing that d is the natural parameter for an external tuning through.

So the special problem of one pulse on a linear fiber can be reduced to a single implicit equation.

An example is shown in Figure 9. The phase space plot reveals that the present pulse (Fig. 9a δ)

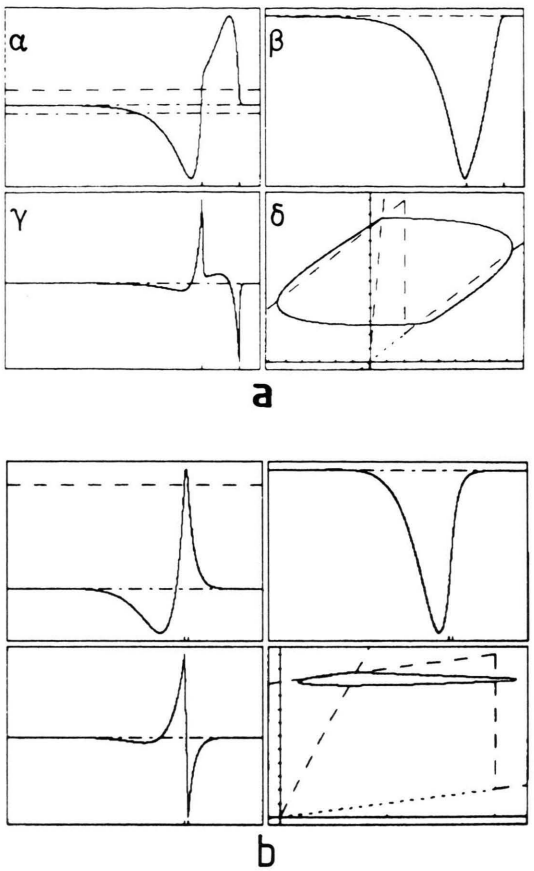

Fig. 9. Single stable (a) and unstable (b) pulse on a linear fiber moving from left to right. In (α), (β), and (γ) the wave variable ξ is plotted versus the system variables u, v, and w, respectively. The ($-\cdot-$) level lines indicate the steady state values while the ($---$) line in (α) shows the excitation threshold d. In (δ) the pulse is projected into the state space (u, -space) of the local reaction system (in the following, this representation of a wave solution will be used several times). *Parameters:* $b = 1$, $d = 0.2$, $e = 15$, $\mu = 100$.

is a trigger wave (cf. Introduction): Diffusion gives only the starting stimulus (that heaves the system over the threshold), but thereafter the system behaves most like a local system completely decoupled from its neighbors.

Figure 10 shows how the propagation velocity of the single impulse depends on the excitation parameter d. This picture was obtained by calculating about 300 impulse solutions of (48), where the λ_i and $\mathbb{H}_{ij}$ were obtained using (17–19).

Figure 10 shows two things: (i) Wave solutions only exist in a finite interval $(d_{\min}, d_{\max}]$ of the excitation parameter d. (ii) In the region of existence, there always exist two solutions of (48) except for the "knee" of the curve.

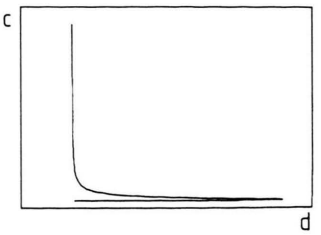

Fig. 10. Propagation velocity c of a single pulse as a function of the excitation parameter d. The upper branch shows the fast, stable pulse solutions while the lower branch represents the unstable, slow pulses. *Parameters:* $b = 1$, $e = 15$, $\mu = 100$. *Axes:* $d = 0.0 \ldots 0.4$, $c = -40 \ldots 1100$.

The first result is in accordance with an estimate to be obtained from the local system. Here a lower bound below which no wave solution can be supported is given by condition (ia) of Sect. 2, which yields

$$d^{\mathrm{l}}_{\min} = b/(e-1); \tag{49}$$

here the superscript "l" indicates the local results.

For the upper bound, one obtains analogously

$$d^{\mathrm{l}}_{\max} = \frac{b\,e}{e-1} - b + 1 \tag{50}$$

since for $d > d^{\mathrm{l}}_{\max}$ no stimulus pointing in the u-direction can lead to a fast relaxation into a neighborhood of the lower branch of the u-nullcline. If now diffusion is added, $d_{\max}$ is bound to be smaller than $d^{\mathrm{l}}_{\max}$ because of the additional outflow provided by diffusion.

The second result (point 2 above) is harder to see intuitively. The weakly coupled waves (trigger waves of Fig. 9) are all represented by the upper branch of Figure 10. The lower branch corresponds to a second type of waves. These slower pulses are of smaller amplitude. They are "strongly coupled waves": the kinetics and the diffusion almost balance each other as far as their influence on the local behavior is concerned. This second type of waves is always unstable [16].

As a third result Fig. 10 shows that while the slower wave velocity on the lower (unstable) branch of the dispersion relation remains virtually constant, the velocity of the faster pulse strongly diverges on the upper branch as d approaches $d_{\min}$. This too follows from a glance at the local system: the differ-

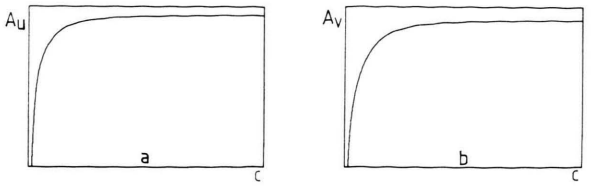

Fig. 11. Amplitudes of the system variables u (a) and v (b) as functions of the wave velocity for a single pulse on the linear fiber. *Parameters:* $b = 1$, $e = 15$, $\mu = 100$. *Axes:* a) $c = 0 \ldots 200$, $A_u = 0.0 \ldots 1.7$; b) $c = 0 \ldots 200$, $A_v = 0.0 \ldots 1.1$.

ence $(d - d_{\min})$ plays the role of an excitation parameter. As d approaches $d_{\min}$, the upper stable steady state is about to disappear (and oscillatory behavior about to appear). Shortly before this happens, the "reaching distance" of diffusion (determining the velocity of propagation) becomes arbitrarily large since very small diffusion fluxes are now sufficient for excitation (cf. also [1, 2]).

A final result shows the dependence of wave amplitudes on propagation velocity. In Fig. 11, the amplitudes of the wave solutions of (48) were plotted versus propagation velocity. Both amplitudes asymptotically approach the amplitude of excitation of the local system as c becomes larger and larger. Thus more and more ideal trigger-wave behavior occurs.

9. Single Pulse on the Ring

In the case of one pulse on the linear fiber (preceding Section), only a single interval length had to be obtained. Therefore the implicit system of algebraic equations (29) could be reduced to just one implicit equation. In all other cases, including

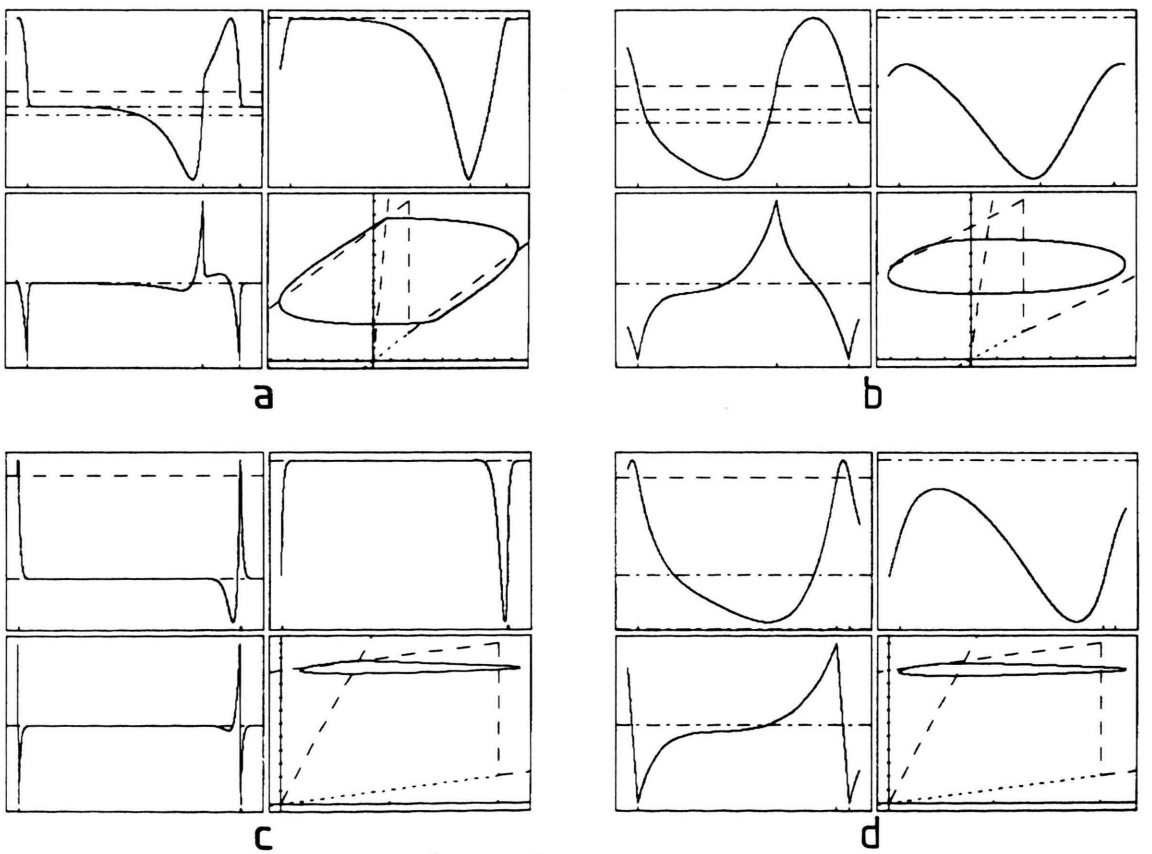

Fig. 12. Single pulses on a ring fiber. The plot ends exhibit an overlap of about 5%, so the figures show just one pulse. In (a) a stable pulse is shown on a long ring, so the pulse looks much like one on a linear fiber. In (b) a stable pulse is shown on a ring close to the minimal ring length. In (c) and (d) the same situations are demonstrated for unstable pulses. *Parameters:* $b = 1$, $d = 0.2$, $e = 15$, $\mu = 100$.

the present problem, the solution of (29) or (37), respectively, has to be obtained by solving at least two implicit equations simultaneously. Programs for the practical evaluation of zeros of systems of algebraic equations are available (cf. [17]).

Figure 12 shows the shape of a single impulse on the ring (which is similar to Figure 9). The behavior is again very close to that of a purely local excitation if the ring is long. Shortening the ring means that no point on the circumference can regenerate completely, so the next excitation reaches the same point when it still is in a relative refractory state. This effect is shown in Figure 12 b.

When the ring is shortened further, the stable pulse disappears (at $\Phi = 0.5707$), meaning that the pulse of Fig. 12 b is relatively close to this threshold. Figure 13 shows the dependence on the ring length quantitatively. One sees that two pulses are possible on the ring (stable and unstable) with pulse velocity plotted versus ring length in Fig. 13 a, and pulse frequency as a function of the length in Figure 13 b. There is not only an asymptotically approached maximum propagation velocity (the velocity found on the linear fiber) for large ring lengths (upper branch of Fig. 13 a), but there also exists a *minimum* ring size, below which no pulse exists.

As the ring is shortened progressively, the stable pulse slows down because of increasing self-repulsion (upper branch of Figure 13 a). This effect is less than proportional to the decrease in ring length – as the progressive increase in slope in the left-hand part of Fig. 13 a shows. As a consequence, pulse frequency increases (upper branch of Figure 13 b).

Analogous arguments hold true for the unstable pulses (lower branch of Figs. 13 a and 13 b).

That a maximal pulse frequency exists follows already from a look at the local system. When we conceive of the whole dynamics of the system as a sequence of jumps alternating between the two branches of the u-nullkline, then the maximum frequency $\nu_{\max}$ is the inverse of the time needed for one jump back and forth. This time is strongly determined by the stiffness parameter μ. The relaxation time of stiff systems is smaller and hence the frequency is larger than that of more slowly relaxing ones.

So far, the parameter d was kept constant. If we again vary it (as was done on the linear fiber, Fig. 10), we obtain a *dispersion hyperplane* in Φ,c,d-space. Figure 14 shows some representative cuts through this surface. Note that the surface continues to the left up to arbitrarily long ring lengths Φ.

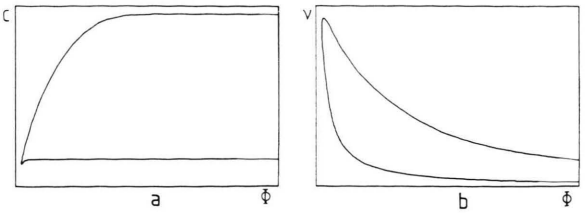

Fig. 13. Propagation velocity c (a) and pulse frequency ν (b) as a function of ring length Φ. The upper branch in each case represents stable pulses while the lower one represents unstable pulses. *Parameters:* $b = 1$, $d = 0.2$; $e = 15$, $\mu = 100$. *Axes:* a) $\Phi = 0 \ldots 25$, $c = 0 \ldots 23$; b) $\Phi = 0 \ldots 25$, $\nu = 0 \ldots 6$.

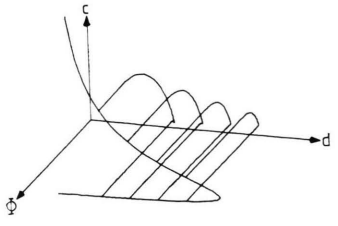

Fig. 14. Dispersion hyperplane of a single pulse on a ring fiber in Φ,c,d-space. *Axes:* $\Phi = 0 \ldots 25$, $c = 0 \ldots 33$, $d = 0.0 \ldots 0.4$.

10. Wave Trains

The present theory is not restricted to single pulses. It can be used to yield results for finite wavetrains of arbitrary length. In practice, the requisite computer memory and time increase faster than linearly with the number of pulses. This is a consequence of the high dimensionality of state space (spanned by c, d, and the φ_i of (29) or (37), respectively). Therefore, explicit dispersion relations can be calculated only for relatively short wavetrains.

If there is more than one pulse, new effects appear. On both the linear and the ring fiber, the stable (upper) branch of the dispersion relation shows less structure (more symmetry) than the unstable (lower) one (see Figs. 10 and 13 a, respectively).

Let us first look at stable pulses on the linear fiber. The first stable pulse will be hardly (if at all) affected by subsequent pulses (in consequence of the weak coupling assumed). It moves into the

steady state region with its "natural velocity" c_0. Every point on the fiber behind the first pulse tries to reapproach the steady state. Whenever the steady state $\bar{L}$ is a node, a second excitation is therefore bound to experience a higher threshold compared to the first one*. In this case the second pulse and further pulses travel more slowly than the first one: they "feel" a repulsive force exerted by the preceding pulse. This repulsion decays more or less exponentially but vanishes only for infinite distances. As a consequence, any wavetrain spreads out and never achieves a constant shape in finite time. This explains why no more than a single stable pulse governed by a node is possible on the linear fiber.

If the steady state $\bar{L}$ is a focus, however, the local state on the fiber necessarily "overshoots"**. This means that a subsequent excitation is facilitated in certain time intervals. Therefore, a second pulse may move faster than c_0 for a while until it comes close enough to the first one for repulsion to set in. In many cases, this adjustment will be monotonic. If there are more than two pulses, however, the adjustment process of the third pulse, depending on two preceding pulses, may as well be nonmonotonic. Whenever this oscillatory process is damped, several stable pulses of different shapes will settle into a wavetrain of constant shape. For a numerical example (based on a different equation), see [18].

This possibility will not occur in the following because only parameters leading to real eigenvalues (solutions of (17)) were to be considered on the stable branch of the dispersion relation. In this case, no more than a single stable pulse can exist on the linear fiber. By the same argument, asymmetric wavetrains of constant shape can be excluded on the ring. Due to the high dimensionality of the parameter space of (13), however (5 parameters: μ, b, c, d, e), we do expect to find also parameter values with complex conjugate eigenvalues that lead to stable multiple (symmetric and asymmetric) pulses.

Let us now turn to *unstable* "symmetric" and "asymmetric" wavetrains. Some examples of symmetric multiple pulses on the linear fiber are given in Figure 15. (Cf. also Table 1.)

"Symmetric" here means that all the pulses have almost the same shape that differs only slightly from the shape of a single pulse (cf. the phase space plots of Figure 15). In addition one sees that the distances between the pulses are "quantized" (cf. [15, 18]), showing a "ground state" (minimum distance between the pulses) and "excited states". In the symmetric part of the lower branch of the dispersion relation (see Fig. 17 below) the ground state and all excited states represent symmetric wavetrains while in the asymmetric part only the excited states yield this type of solution.

More interesting are the asymmetric wavetrains. Cases with ten asymmetric unstable pulses are presented in Figure 16.

There is a large variety of further subtypes (in the grouping of the pulses) that could be presented. Note that in each group, the last (left-most) pulse is the biggest in amplitude; it seemingly "pushes" along the other pulses of the group. Inside a group one finds only the minimum distance between the pulses while the groups are separated by inserted additional "distance quanta".

Figure 17 shows for the linear fiber a segment of the lower (unstable) part of the dispersion relation (cf. Fig. 10b for a d,c-plot). One sees nine (or $N-1$, in the general case) asymmetric branches veering away from the symmetric unstable branch of the dispersion relation.

The lowermost branch is almost the same as for symmetric wavetrains. Coming from above ($d_{\max}$), all branches almost coincide; at $d = 0.333$ the (asymmetric) branches veer away from the lower (symmetric) one. For values further below, the bundle of asymmetric branches decomposes, meaning that the different branches successively diverge until they all are well separated. Approaching $d_{\min}$ all branches again come closer together in order to coincide at $d_{\min}$.

Now the ring fiber. This time, there is no unequivocal "leading" pulse. Only when the wavetrain is well contained is it possible to order the pulses in a convincing way. Examples of unstable asymmetric wavetrains on the ring are presented in Fig. 18 (compare with Figure 16). Here too, many more solutions can be found by grouping the pulses and by inserting additional distance quanta.

A typical dispersion relation on the ring is shown in Figure 19. It shows a segment (the "nose") of Fig. 13a, amplified, for the case of two unstable asymmetric pulses.

This picture is a projection from five-dimensional c,φ-space $(c, \varphi_1, \ldots, \varphi_4)$ onto the c,φ_1-plane,

* (cf. Figure 5b.)

** (cf. Figure 5a.)

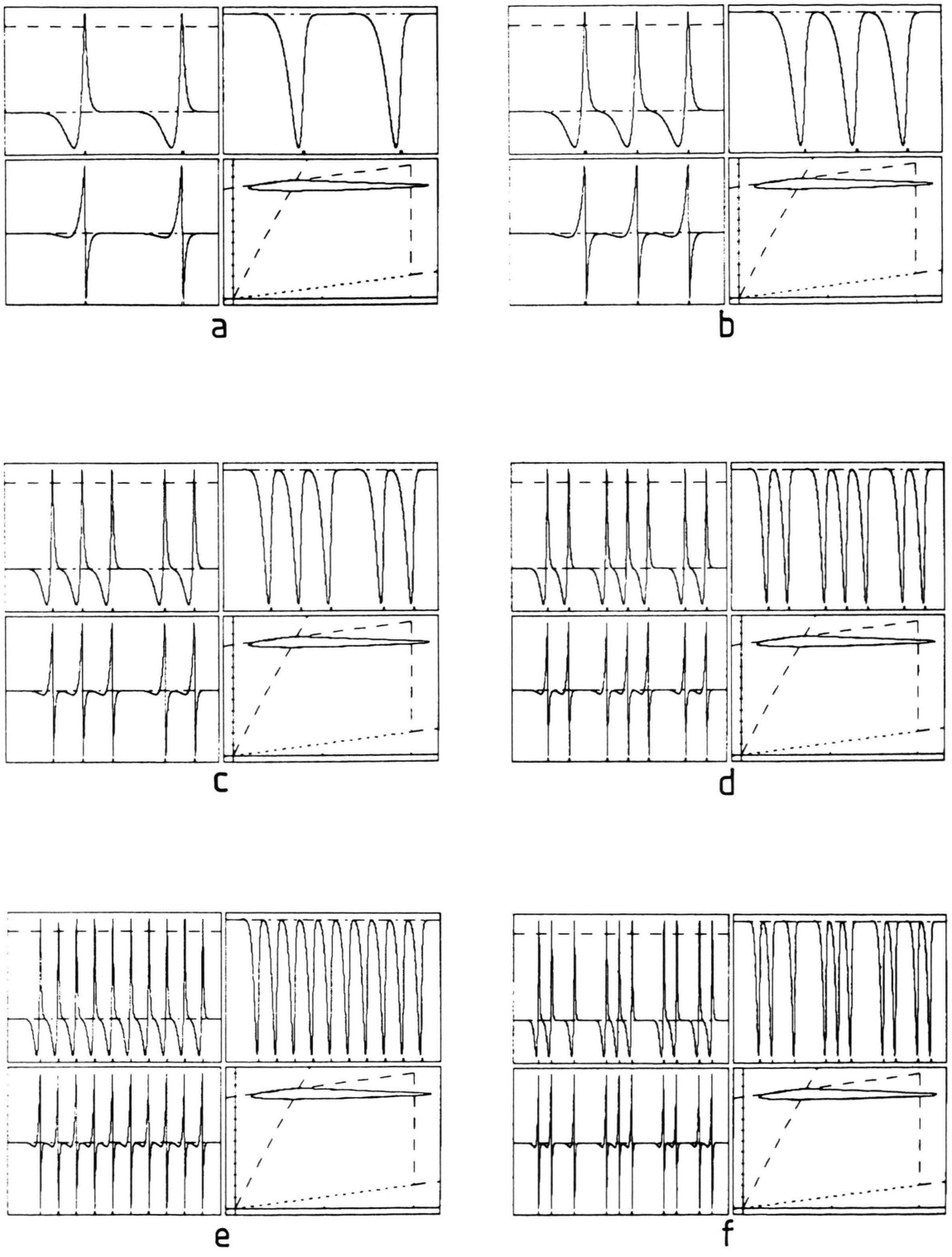

Fig. 15. Examples of symmetric multiple pulses on a linear fiber. Note that in the phase-space plots the single pulses appear indistinguishable. *Parameters:* $b = 1$, $d = 0.2$, $e = 15$, $\mu = 100$.

Table 1. Summary of the numerical results shown in Figs. 9a–b, 12a–d, 15a–f, 16a–f, 18a–d, and 20a–d.

Fig.	9a	9b	12a	12b	12c	12d	15a	15b	15c
d	0.2000	0.2000	0.2000	0.2000	0.2000	0.2000	0.2000	0.2000	0.2000
c	21.975	3.5270	21.905	6.5563	3.5269	3.2528	3.5269	3.5269	3.5269
$\varphi_1/0.1$	0.0000	0.0000	100.00	8.0000	100.00	8.0000	0.0000	0.0000	0.0000
$\varphi_2/0.01$	207.67	4.3770	206.78	41.703	4.3769	4.8992	4.3769	4.3699	4.3699
$\varphi_3/0.1$	–	–	–	–	–	–	27.513	15.286	15.286
$\varphi_4/0.01$	–	–	–	–	–	–	4.3769	4.3699	4.3699
$\varphi_5/0.1$	–	–	–	–	–	–	–	15.284	15.285
$\varphi_6/0.01$	–	–	–	–	–	–	–	4.3769	4.3769
$\varphi_7/0.1$	–	–	–	–	–	–	–	–	27.518
$\varphi_8/0.01$	–	–	–	–	–	–	–	–	4.3699
$\varphi_9/0.1$	–	–	–	–	–	–	–	–	15.285
$\varphi_{10}/0.01$	–	–	–	–	–	–	–	–	4.3769

Fig.	15d	15e	15f	16a	16b	16c	16d	16e	16f
d	0.2000	0.2000	0.2000	0.2000	0.2000	0.2000	0.2000	0.2000	0.1039
c	3.5269	3.5269	3.5269	3.3526	3.3527	3.3810	3.3886	3.3526	2.2314
$\varphi_1/0.1$	0.0000	0.0000	0.0000	0.0000	0.0000	0.0000	0.0000	0.0000	0.0000
$\varphi_2/0.01$	4.3699	4.3699	4.3699	14.948	15.117	4.4601	7.3931	15.155	4.9482
$\varphi_3/0.1$	15.285	15.287	15.284	4.4929	4.5622	11.523	3.4583	4.5789	2.1857
$\varphi_4/0.01$	4.3769	4.3699	4.3769	14.258	15.057	15.229	4.3683	15.260	4.5175
$\varphi_5/0.1$	27.516	15.287	27.518	4.1773	4.4785	4.5065	14.492	4.5655	1.8704
$\varphi_6/0.01$	4.3699	4.3699	4.3769	11.530	14.262	14.509	4.5860	15.261	3.9179
$\varphi_7/0.1$	15.287	15.287	38.292	3.5163	4.1768	4.1733	9.5476	4.5648	1.7174
$\varphi_8/0.01$	4.3699	4.3699	4.3699	7.4584	11.530	11.625	4.5859	15.255	3.3399
$\varphi_9/0.1$	15.285	15.287	15.287	3.2867	3.5162	3.4692	9.5480	4.5622	1.6339
$\varphi_{10}/0.01$	4.3769	4.3699	4.3699	4.3785	7.4584	7.4202	4.5859	15.224	2.8224
$\varphi_{11}/0.1$	27.517	15.287	15.285	25.211	3.2865	3.2289	9.5480	4.5484	1.5959
$\varphi_{12}/0.01$	4.3699	4.3699	4.3769	14.948	4.3784	4.3478	4.5859	15.058	2.3671
$\varphi_{13}/0.1$	15.285	15.287	39.521	4.4929	23.799	16.503	9.5484	4.4782	1.5988
$\varphi_{14}/0.01$	4.3769	4.3699	4.3699	14.258	14.139	7.3873	4.5868	14.261	1.9655
$\varphi_{15}/0.1$	–	15.287	15.284	4.1772	4.1972	3.4699	9.5317	4.1768	1.6520
$\varphi_{16}/0.01$	–	4.3699	4.3769	11.530	11.526	4.3642	4.5469	11.530	1.6050
$\varphi_{17}/0.1$	–	15.287	27.523	3.5163	3.5178	14.105	10.278	3.5163	1.7911
$\varphi_{18}/0.01$	–	4.3699	4.3699	7.4582	7.4581	7.4119	7.4062	7.4582	1.2690
$\varphi_{19}/0.1$	–	15.285	15.284	3.2867	3.2871	3.4666	3.4561	3.2867	2.1632
$\varphi_{20}/0.01$	–	4.3769	4.3769	4.3784	4.3784	4.3825	4.3778	4.3784	0.9257

Fig.	18a	18b	18c	18d	20a	20b	20c	20d
d	0.2000	0.2000	0.2000	0.2000	0.1000	0.1000	0.1000	0.1000
c	3.3917	3.3580	3.3557	3.3700	2.8256	3.0766	3.0766	3.0766
$\varphi_1/0.1$	17.000	19.000	19.000	19.000	0.0000	0.0000	0.0000	0.0000
$\varphi_2/0.01$	7.3973	11.406	14.164	15.073	1.1324	0.7969	0.7987	0.7987
$\varphi_3/0.1$	3.4501	3.5657	4.1976	4.4865	3.1347	13.249	23.572	33.474
$\varphi_4/0.01$	4.3675	7.4508	11.537	14.335	0.7994	0.7987	0.7987	0.7987
$\varphi_5/0.1$	–	3.2942	3.5130	4.1855	–	–	–	–
$\varphi_6/0.01$	–	4.3729	7.4533	11.577	–	–	–	–
$\varphi_7/0.1$	–	–	3.2827	3.4871	–	–	–	–
$\varphi_8/0.01$	–	–	4.3725	7.4498	–	–	–	–
$\varphi_9/0.1$	–	–	–	3.2702	–	–	–	–
$\varphi_{10}/0.01$	–	–	–	4.3663	–	–	–	–

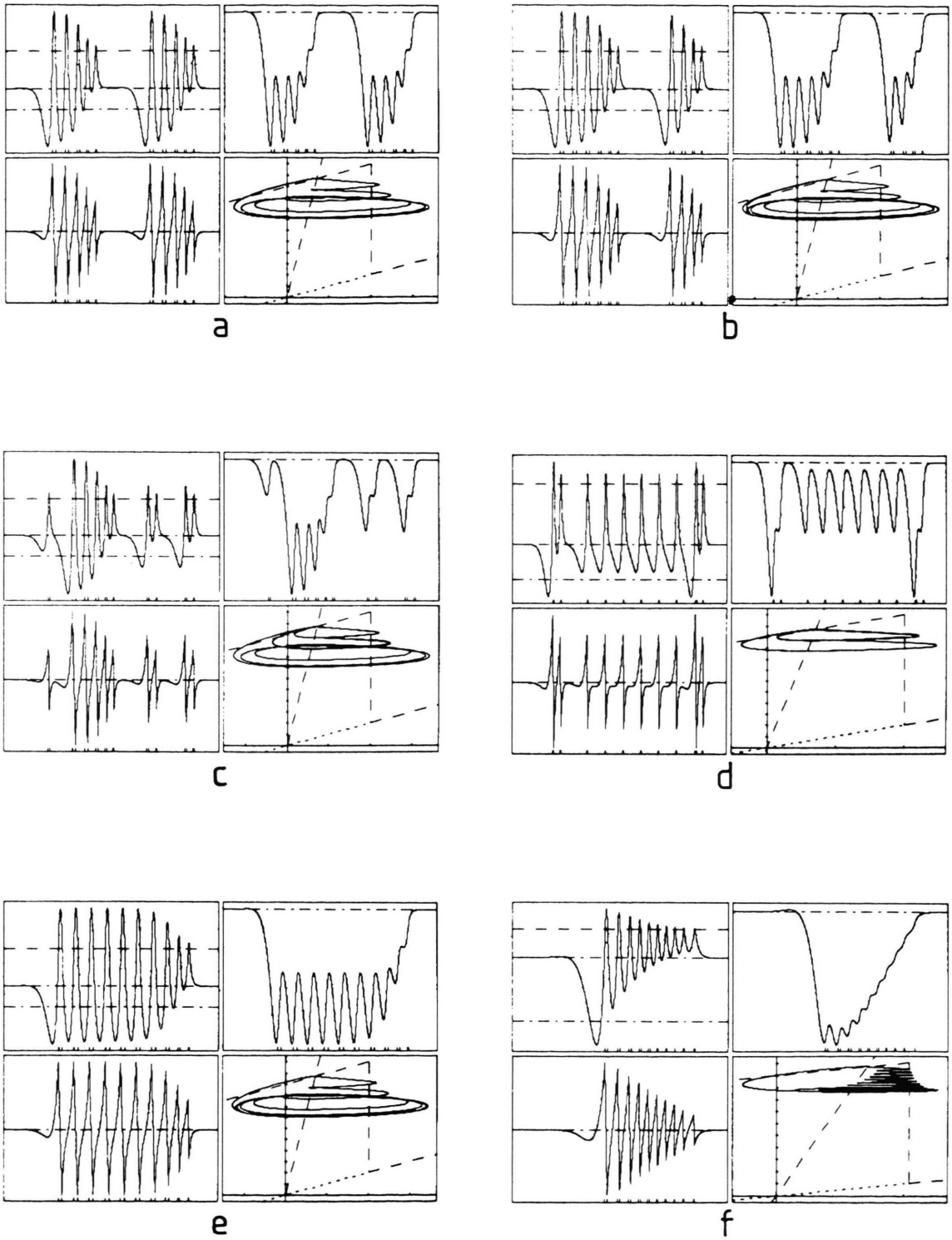

Fig. 16. Examples of asymmetric wavetrains containing ten pulses on a linear fiber. One sees that there is a great variety of grouping the pulses and of arranging the groups. *Parameters:* a) – e) $b = 1$, $d = 0.2$, $e = 15$, $\mu = 100$; f) $b = 1$, $d = 0.1039$, $e = 15$, $\mu = 100$.

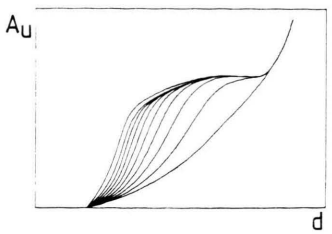

Fig. 17. Dispersion relation for an unstable wavetrain consisting of ten pulses in one group (cf. Fig. 16 e, f). The veering off, higher branches represent the bigger (left-more) pulses of the wavetrain. *Parameters:* $b = 1$, $e = 15$, $\mu = 100$. *Axes:* $d = 0.0 \ldots 0.4$, $A_u = 0 \ldots 0.75$.

or c, φ_3-plane, respectively. The right-hand intersection point is a genuine intersection point in $\mathbb{R}^5$. The other is a projection artifact. The right-hand intersection point is the bifurcation point (having a horizontal tangent in one branch). The dashed curve is the symmetric branch while the lower, solid one represents an asymmetric double pulse for every point. Below $c_i = 2.936$, there exist only symmetric wavetrains (dashed curve). In the interval between $c = 2.936$ and $c = 3.386$, symmetric and asymmetric double pulses coexist, while above that interval, only symmetric solutions remain. Thus, symmetric pulses can be both faster and slower than asymmetric ones.

10. Discussion

Many interesting features of nonlinear reaction diffusion systems can be obtained from "few region" piecewise linear systems. These systems form a kind of prototype for the whole class. The modified Rinzel-Keller system considered above is a "two region" model. Here all excitation characteristics of the imbedding medium are condensed into one parameter d. The second important parameter, the "stiffness parameter" μ, was kept constant a $\mu = 100$.

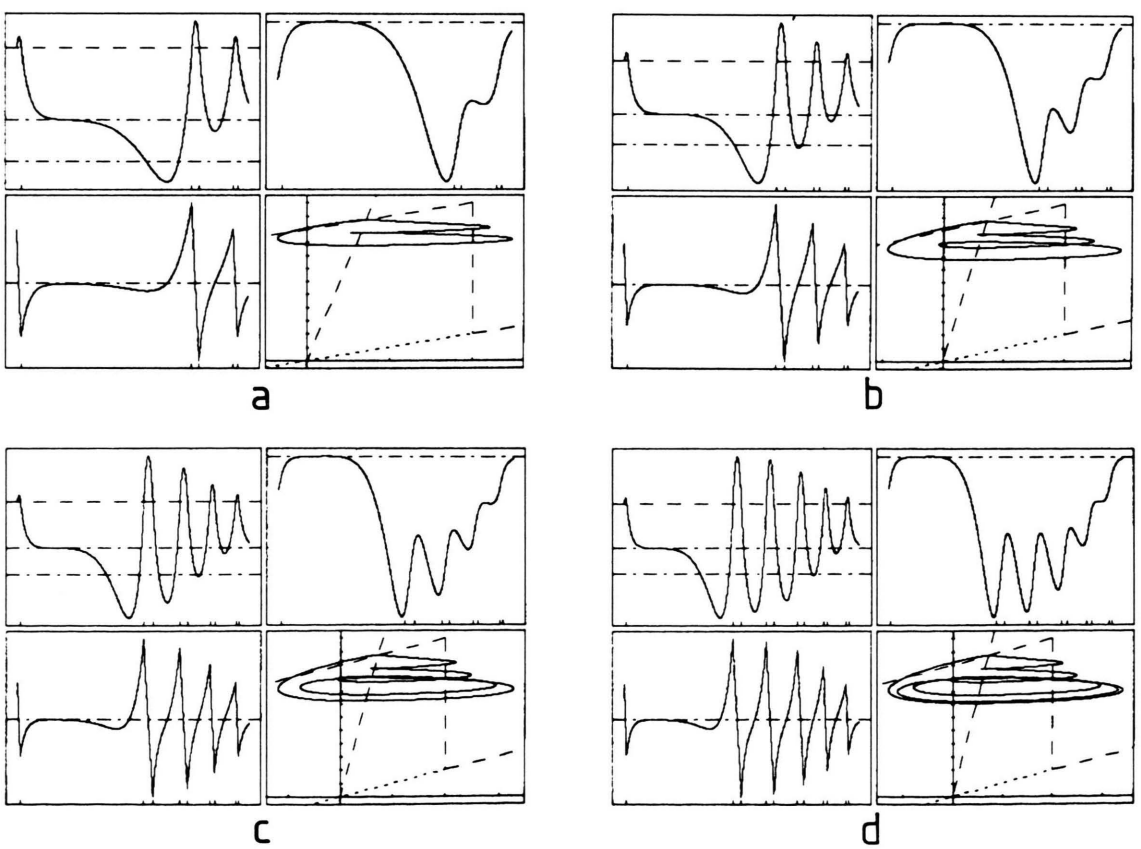

Fig. 18. Asymmetric wavetrains of 2, 3, 4 and 5 pulses in one group on the ring fiber. *Parameters:* $b = 1$, $d = 0.2$, $e = 15$, $\mu = 100$.

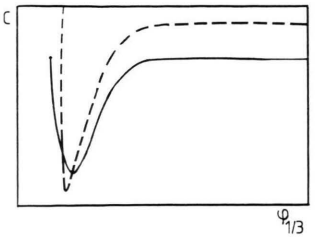

Fig. 19. Dispersion relation for an asymmetric double pulse on a ring fiber. The dashed line represents the symmetric pulses (cf. the "nose region" of Fig. 13a) while the solid line represents asymmetric double pulses. *Parameters:* $b=1$, $d=0.2$, $e=15$, $\mu=100$. *Axes:* $\varphi_{1/3}=0\ldots3$, $c=2.8\ldots3.6$.

In principle, there exist two ways for calculating the solutions of a piecewise linear system: the "sequential" and the "simultaneous" method. In the first method, the solutions are calculated sequentially, with the final value of the last interval taken as the starting condition for the next one. This requires the successive solution of a single-variable implicit equation. In this case, the desired solution is found by varying a single parameter, c for the linear fiber, or by varying two parameters (e.g. η_1^1 and Re η_2^1) for the ring. However, this straightforward approach in practice reveals several severe shortcomings. They stem from the fact that as more and more impulses are being considered, all the numerical errors accumulate in the one (or two) variational parameters on hand. In addition, differing solutions may come to lie so close together in the low dimensional space of variational parameters as to be no longer distinguishable.

The second method, used above, is the "simultaneous" method. As Sects. 5 and 6 show, it requires a little bit more machinery, but it lacks the above cited shortcomings in return. It provides good results as long as the different solutions are well separated in just one of the $2N$ (on the linear fiber) or the $2N+1$ (on the ring fiber) variational parameters in c,φ-space that are now available. Note that N is the number of impulses within the wavetrain to be considered.

Feroe [10] found only two different solutions of the double pulse problem (using a 23-digit accuracy). The present method allows to find more (see Fig. 20, which was computed with 12-digit accuracy).

Two major phenomena concerning wavetrains of two or more pulses could be investigated for the first time: the dependence of their propagation on changes in the local excitability (parameter d) on the one hand, and on variations of geometry (ring length) on the other. On the linear fiber, the natural parameter to "tune through" was d. On the ring fiber it was ring length (while d was kept constant, except for Fig. 14 where both parameters were varied).

In either case two types of solutions were found: (1) stable pulses of high propagation velocity, and (2) unstable wavetrains that were slow in general (Figure 13a). The stable pulses were called "weakly coupled"

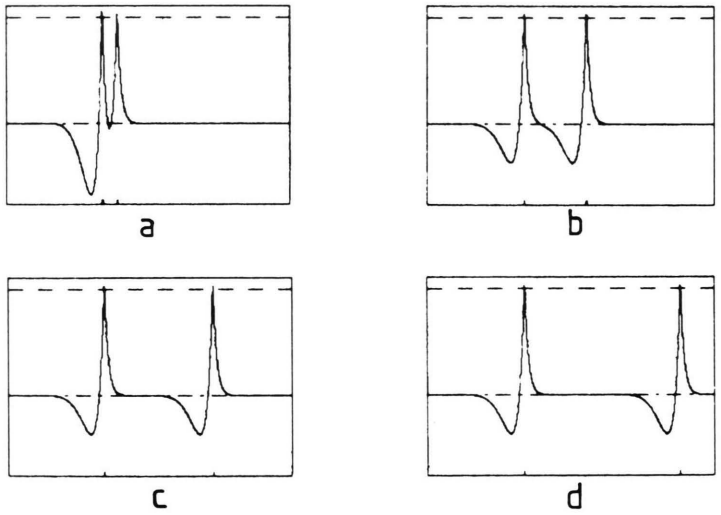

Fig. 20. Four different solutions of the double pulse problem, showing the ground state and the first three excited states of a double pulse. In each case the u-component is plotted versus ξ in the same scale.

(or trigger waves) since the shapes of their trajectories when projected into the phase space of the local system appeared almost like excitations of that reaction system. The slow unstable pulses, in contrast, were called "strongly coupled" since the influences of diffusion and reaction were found to be of similar strength. This is virtually equivalent to having an additional new reaction path introduced into the system. This might be the explanation why a larger variety of phenomena was found for this type. All the asymmetric wavetrains described in Figs. 16 and 18 are new findings. The dispersion relation of Fig. 17 (with the "veering off" of subpulses) as well as the asymmetric dispersion relation on the ring (Fig. 19) are also new findings.

All results reported here were found under the assumption of constant shape and finite length of all wavetrains. Dropping the first constraint is no longer compatible with formulating the problem as an ODE, but will allow one to investigate not only transient phenomena, but also oscillations in c,φ-space (that is, pulsating wavetrains). Dropping the second assumption, in contrast, merely implies a change of boundary conditions. In this case, truly nonperiodic wavetrains (with an infinite number of pulses) can be expected to be found analytically by an extension of the above method.

C. Kahlert wants to thank the Studienstiftung des deutschen Volkes for supporting this work.

[1] A. T. Winfree, The Geometry of Biological Time, Springer-Verlag, New York 1980.
[2] O. E. Rössler and C. Kahlert, Z. Naturforsch. **34 a,** 565 (1979).
[3] P. C. Fife, Mathematical Aspects of Reacting and Diffusing Systems, Springer-Verlag, New York 1979.
[4] A. L. Hodgkin and A. F. Huxley, J. Physiol. **117,** 500 (1952).
[5] K. F. Bonhoeffer, Naturwiss. **31,** 270 (1943).
[6] R. FitzHugh, Biophys. J. **1,** 445 (1961).
[7] J. Nagumo, S. Arimoto, and S. Yoshizawa, Proc. IRE **50,** 2061 (1962).
[8] J. Rinzel and J. B. Keller, Biophys. J. **13,** 1313 (1973).
[9] C. Kahlert, Dispersionsrelationen für eine Klasse von Reaktions-Diffusions-Gleichungen, Thesis, Tübingen 1981.
[10] J. A. Feroe, SIAM J. Appl. Math. **42,** 235 (1982).
[11] C. W. Gear, Numerical Initial Value Problems in Ordinary Differential Equations, Englewood Cliffs, Prentice-Hall, London 1971.
[12] P. J. Davis and P. Rabinowitz, Numerical Integration, Blaisdell Publishing Company, Waltham (Massachusetts), Toronto 1967.
[13] M. W. Hirsch and S. Smale, Differential Equations, Dynamical Systems, and Linear Algebra, Academic Press, New York 1974.
[14] W. D. Jackson, Classical Electrodynamics (Second Edition), John Wiley and Sons, New York 1975.
[15] J. W. Evans, N. Fenichel, and J. A. Feroe, SIAM J. Appl. Math. **42,** 219 (1982).
[16] J. Rinzel, Biophys. J. **15,** 975 (1975).
[17] M. J. D. Powell, A FORTRAN Subroutine for Solving Systems of Nonlinear Algebraic Equations, in: Numerical Methods for Nonlinear Algebraic Equations (P. Rabinowitz, Editor), Gordon and Breach Science Publishers, London 1970.
[18] H. R. Karfunkel and C. Kahlert, J. Math. Biol. **4,** 183 (1977).